Processing and Application of Ceramics 19 [4] (2025) 396–407
https://doi.org/10.2298/PAC2504396C

Development of deep potential models for silicon carbide and investigation of damage evolution mechanisms

Tao Chen [1,2,#], Peng Peng Zhang [1,2,#], Xue Zhou Luo [1,#], Chao Bao[1,2], Zeng Guang Lai[1,2], Jian Bo Le[1,2,*]

[1]*School of Mechanical and Electronic Engineering, Jingdezhen Ceramic University, Jingdezhen 333403, Jiangxi, China*
[2]*Laboratory of Ceramic Material Processing Technology Engineering, Jiangxi province, Jingdezhen 333403, Jiangxi, China*

Received 17 September 2025; Received in revised form 6 December 2025; Accepted 12 December 2025

Abstract

Traditional empirical interatomic potentials exhibit limited accuracy in describing the high-temperature structural response of silicon carbide (SiC), while first-principles simulations remain computationally expensive. In this work, a deep neural network interatomic potential for SiC was constructed based on the density functional theory (DFT) datasets. An attention-enhanced descriptor was introduced to improve the representation of bond-length and bond-angle correlations. A concurrent learning workflow based on the deep potential generator (DP-GEN) was employed to iteratively refine sampling of defect configurations and improve force prediction accuracy. The final deep potential model demonstrates close agreement with DFT, achieving root-mean-square errors of 0.42 meV/atom for energy and 49 meV/Å for force. Molecular dynamics (MD) simulations using the developed potential significantly outperform DFT in efficiency, reaching 34 steps per second at 1300 K. Structural evaluation shows that the model reproduces radial distribution characteristics and suppresses high-frequency atomic fluctuations at elevated temperatures. Nano-indentation simulations further reveal temperature-accelerated bond breaking, local structural disorder and expansion of subsurface damage regions. The proposed potential enables reliable atomistic modelling of SiC under severe thermomechanical conditions, providing support for understanding high-temperature damage evolution and extending machine-learning-based simulation of complex processing environments.

Keywords: *SiC, interatomic potential, first-principles, deep learning, damage evolution mechanism*

I. Introduction

Silicon carbide (SiC) serves as a third-generation wide-bandgap semiconductor material [1,2]. It exhibits high hardness, high thermal conductivity, excellent high-temperature resistance and strong irradiation tolerance. Its applications span aerospace, nuclear energy, optoelectronics and advanced manufacturing [3,4]. SiC-based composites are regarded as ideal materials for high-performance structural and friction components. They are endowed with high strength, high modulus and good thermal stability [5–7]. However, silicon carbide exhibits strong brittleness and a complex crystal structure. Microcrack initiation and propagation are easily observed under extreme conditions, such as high-temperature and high-speed grinding. The service life and stability of the material are severely affected [8–10]. Therefore, the damage evolution mechanism at high temperature is investigated at the atomic scale. Its study is regarded as having significant theoretical value and engineering significance for material performance optimization and failure prediction.

Molecular dynamics (MD) is regarded as an important method for studying atomic behaviour in materials. Microscopic structural evolution during grinding is effectively captured. The underlying damage mechanisms are also revealed with its assistance. The accuracy of MD simulation is determined by the modelling of in-

*Corresponding author: +86 13705187680
e-mail: *jelfptocm_ljb@163.com*
#Co-first authors - contributed to the work equally

teratomic interaction potentials. Although atomic interactions are described with high precision by *ab initio* molecular dynamics (AIMD) based on the density functional theory (DFT), an extremely high computational cost is encountered. Large-scale and long-time simulations are therefore difficult to perform [11]. Traditional empirical potentials, such as Tersoff and REBO, are limited in accuracy when describing many-body interactions, interfacial behaviour and non-equilibrium processes at high temperature. They cannot satisfy the simulation requirements for complex friction and wear processes. In recent years, deep learning potentials (DP) trained with first-principles data are regarded as a new generation of interatomic potentials. In this way, accuracy and computational efficiency are balanced [12–14]

To address the insufficient prediction capability of existing potentials for SiC damage evolution under high-temperature grinding, a silicon carbide dataset is constructed in this work based on the first-principles calculations. An attention mechanism is introduced to optimize the structure of atomic environment descriptors. A high-precision deep learning potential model for high-temperature grinding is built using the Deep Potential Molecular Dynamics framework (DeepMD-kit) [15]. The model is gradually improved in generalization and stability under different thermodynamic conditions through adaptive sampling and iterative optimization using DP-GEN [16]. A deep potential model suitable for high-temperature SiC is ultimately constructed. Training results show that the root mean square errors (RMSE) of atomic energy and interatomic force predictions are close to DFT accuracy. Computational efficiency is significantly enhanced. Excellent scalability and practicality are achieved.

Based on the constructed deep-learning potential, atomic-scale molecular dynamics simulations are conducted under high-temperature grinding conditions. The microscopic mechanisms of grinding load evolution, damage region expansion, structural relaxation and fracture behaviour are systematically analysed. High temperature is found to accelerate atomic slip, bond breaking and local structural disorder. Significant expansion of damage regions is observed. The essential effect of temperature increase on subsurface damage evolution in silicon carbide is revealed. This work provides theoretical support for understanding the failure mechanisms of SiC under extreme processing conditions. It also offers guidance for developing machine learning potentials suitable for complex multi-field coupled systems.

II. SiC structure sampling and dataset design

2.1. Structure sampling strategy and DFT computation workflow

During the training of deep learning potentials, the accuracy of the potential depends on the rationality and diversity of the dataset. The rationality of the initial silicon carbide configuration is ensured before the construction of the dataset. The geometric configuration of the initial structure is optimized to obtain the accurate spatial positions of silicon carbide atoms. The detailed process of reconfiguring the atomic spatial positions is shown in Fig. 1.

As shown in Fig. 1a, the construction process of the initial structural positions of silicon carbide atoms is presented. The SiC unit cell contains 18 atoms. A $2 \times 2 \times 2$ supercell expansion is performed in the UNIT CELL module of the VESTA [17] software. After expansion, the crystal size is $x = 8.70799$ Å, $y = 8.70799$ Å, $z = 8.70799$ Å. The total number of atoms in the system reaches 95. A tetrahedral structure is randomly selected in the crystal structure. The bond angle θ_{C-Si-C} is measured as 108.231°. The standard bond angle of 3C-SiC was reported as $\theta_{C-Si-C} = 109.47°$ (ideal tetrahedral angle) by Rino *et al.* [18]. A significant deviation is observed between the current value and the experimental value. The deviation is caused by atomic overlap and spatial site distortion after supercell expansion. Geometric optimization is required before AIMD simulation. The GEO_OPT module of CP2K software is used to optimize the supercell structure. The main algorithms include BFGS, LBFGS and CG. The LBFGS algorithm is memory efficient and is used for very large systems. The CG algorithm is stable for sparse systems but is slow. The BFGS algorithm is suitable for medium systems and converges fast. Therefore, the BFGS algorithm is selected to optimize the initial SiC crystal structure (see Fig. 1b). The convergence criteria are defined. The maximum displacement (MAX_DR) is required to be less than 0.003 bohr ($\approx$ 0.0016 Å). The maximum force (MAX_FORCE) is required to be less than 0.00045 a.u./bohr ($\approx$ 0.00023 eV/Å). The root mean square displacement (RMS_DR) is required to be less than 0.0015. The root mean square force (RMS_FORCE) is required to be less than 0.0003. All four criteria must be satisfied. Otherwise, the iterations are continued until convergence. A complete crystal structure model is obtained after convergence (see Fig. 1c). The bond length distribution of the optimized crystal model is analysed. The average C–Si bond length is measured as 1.885 Å. The value is highly consistent with the experimental value of 1.888 Å reported by Islam [19]. The C–Si–C bond angle and the Si–C–Si bond angle of 3C-SiC are the same. The average bond angle θ_{C-Si-C} is measured as 109.831° after optimization. The value is compared with the experimental value of 109.47° reported by Bekaroglu *et al.* [20]. The error is within the acceptable range. The reconstructed atomic spatial structure is proved to be reasonable. Now the structure can be used as the training dataset for the deep learning potential.

The structural construction stage yields two finalized outputs: i) the optimized periodic SiC crystal structure exported as a standard CIF file containing full lattice and symmetry information and ii) the converged atomic coordinate matrix recorded after geometry relaxation.

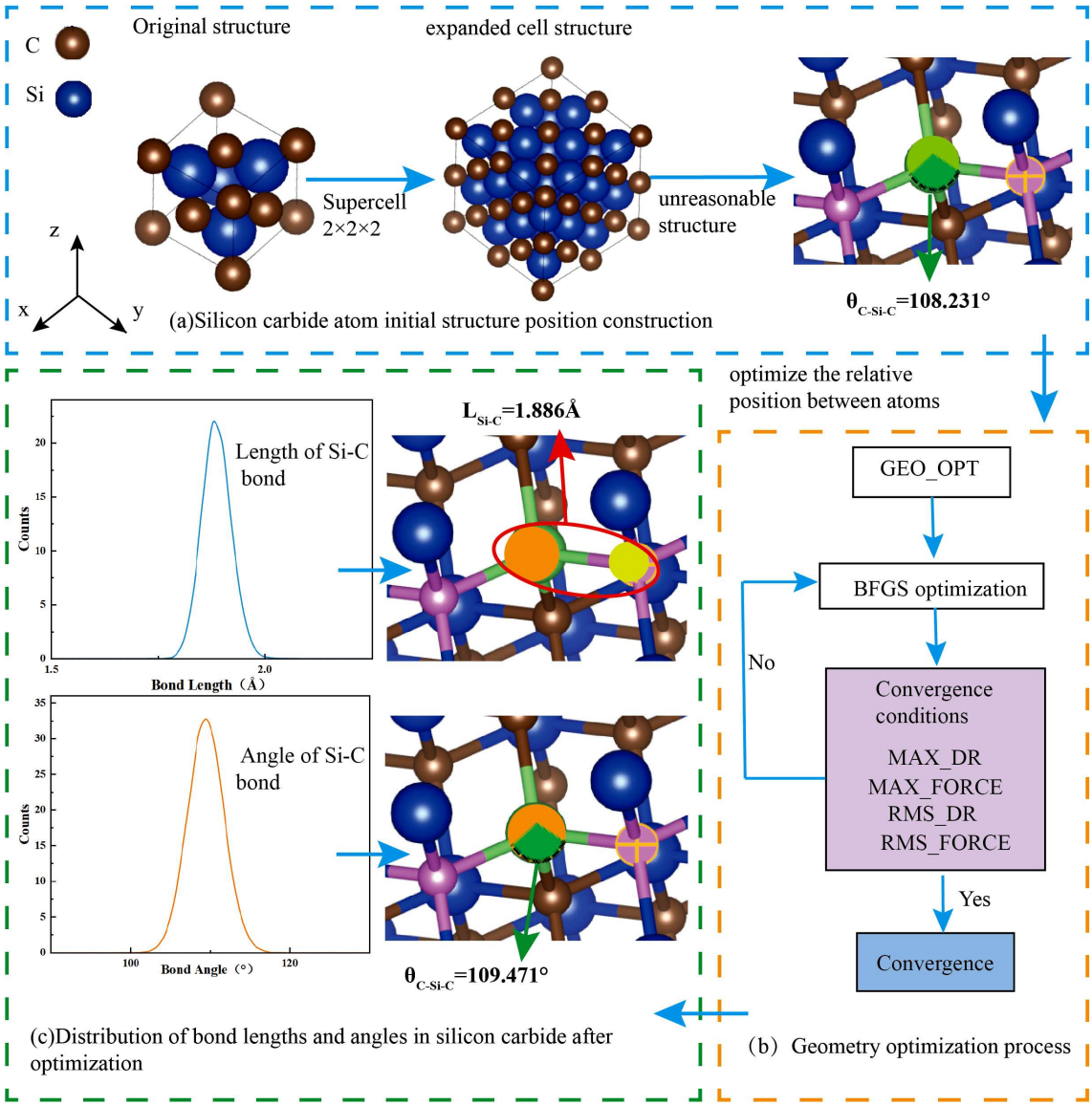

Figure 1. Construction process of the SiC dataset

The CIF file maintains crystallographic periodicity for subsequent structural referencing, whereas the coordinate matrix serves as the explicit numerical basis for descriptor encoding in Deep Potential fitting and DP-GEN adaptive sampling in the next stage.

III. Attention mechanism descriptors

While a sufficiently large dataset is obtained, a reasonable neural network architecture is constructed based on the deep potential to fit the interatomic potential accurately. The fitting process is performed to ensure high precision of the potential. The deep learning potential fitted with the Se_e2_a descriptor alone captures bond angle information insufficiently. Large errors are observed in predicting the physical structure of 3C-SiC. The deep learning potential fitted with the Se_e2 descriptor alone captures bond length information insufficiently. The network structure is too complex. Computational efficiency is significantly reduced. Therefore, attention mechanism descriptors are introduced as shown in Fig. 2.

Figure 2a shows that in covalent materials such as silicon carbide, structural distortion occurs easily if the deep learning potential lacks explicit control of local geometric structures and physical consistency constraints. Consequently, the physical realism and predictive reliability in downstream molecular dynamics simulations could be affected. To construct a high-precision and highly generalizable potential model, effective mechanisms for describing and controlling local geometric information, such as bond lengths and bond angles, are systematically introduced at multiple levels, including model architecture, training strategy, data generation, and physical priors. In Fig. 2b, distances between atom pairs (bond lengths) are described in SE_E2_A using symmetry functions similar to the Behler-Parrinello type or radial basis functions in message passing neural

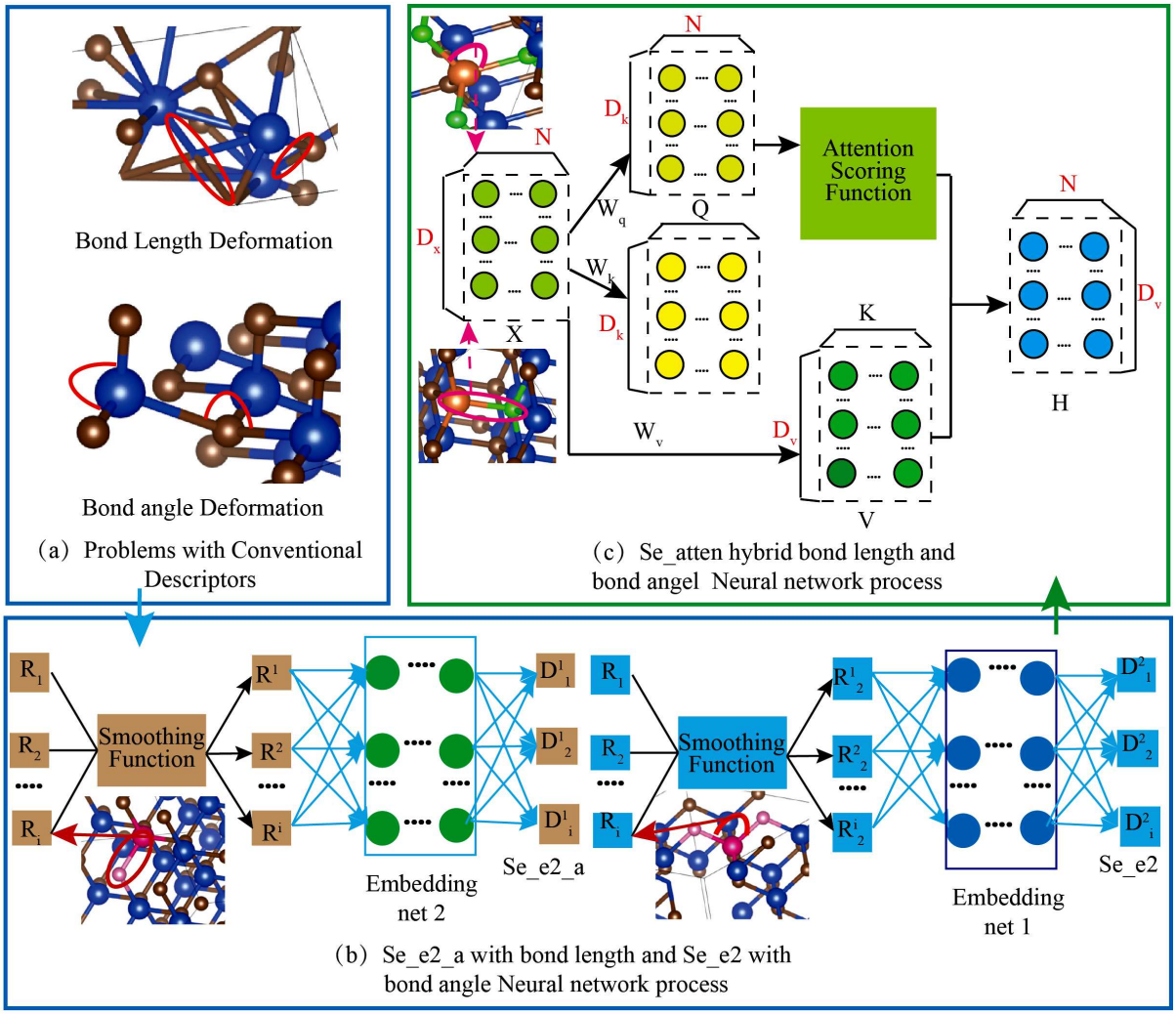

Figure 2. The neural network workflow of the SiC deep learning potential

networks. These functions are usually expressed in the following form:

$$G_i^R = \sum_j e^{-\eta(r_{ij}-R_s)^2} f_c(r_{ij}) \tag{1}$$

where r_{ij} is the distance between atom i and its neighbouring atom j. The cut-off function f_c is used to limit the interaction range. η and R_s control the centre and width of the radial distribution. This descriptor is sensitive to changes in interatomic distances. The potential energy variation caused by local bond stretching is effectively captured. SE_E2_A mainly introduces two-body radial descriptors. They only reflect the distance distribution between atom pairs. Bond angles in three-atom configurations cannot be represented. Therefore, bond angle distortion occurs easily. In SE_E2, angular descriptors are represented by angular features expanded with spherical harmonics. They show excellent directional sensitivity. However, radial information, such as bond lengths or distances, are not represented sufficiently or independently. The atomic environment in SE_E2 is encoded through spherical harmonic expansion as follows:

$$\rho_i(r,\theta,\phi) = \sum_j f(r_{ij}) \cdot Y_{lm}(\theta_{ij},\phi_{ij}) \tag{2}$$

where Y_{lm} represents the spherical harmonics and encodes directional angle information. $f(r_{ij})$ represents the distance function, which usually uses radial basis functions such as Bessel or Gaussian. The spherical harmonics $Y_{lm}(\theta,\phi)$ are independent of distance and sensitive only to angles. If the radial function part is simplified during descriptor construction, the distinction of different bond length configurations in the high-dimensional embedding space is poor. In Fig. 2c, bond lengths and bond angles are included as descriptors in the self-attention mechanism. This approach allows the attention mechanism to identify and weight local geometric information. The model becomes more sensitive to changes in local configurations, including bond lengths and bond angles, and the physical modelling ability is enhanced. The input is provided as a feature matrix of the atomic structure:

$$\left[X \in R^{N\times D_X}\right] \tag{3}$$

The bond length between atoms i and j is defined as r_{ij}. The bond angle formed by atoms i-j-k is defined as θ_{ijk}. G_{ij} and r_{ij} are encoded as structural descriptors θ_{ijk}. In the first step, queries, keys, values, $Q = XW_q$, $K = XW_K$ and $V = XW_V$ are generated as in the standard self-attention. W_q, W_K and W_V are trainable weight matrices. In the second step, structure-aware bias terms are constructed. Bond lengths and bond angles are embedded to introduce geometric bias information B_{ij}. The geometric bias can be defined as follows:

$$B_{ij} = \emptyset_r(r_{ij}) + \emptyset_\theta(\theta_{ijk}) \tag{4}$$

where $\emptyset_r(r_{ij})$ represents the bond length embedding function, such as the radial basis function expansion. $\emptyset_\theta(\theta_{ijk})$ represents the bond angle embedding function, such as angle encoding or many-body tensor. In the third step, structure-aware attention scores are calculated. The attention score calculation formula is modified to include structural information:

$$\bar{A}_{ij} = \frac{Q_i K_j}{\sqrt{D_K}} + B_{ij} \tag{5}$$

B_{ij} controls whether the attention focuses on distant atoms or non-ideal angles. In the fourth step, attention weights are normalized using the *softmax* function:

$$A_{ij} = softmax_j(\bar{A}_{ij}) = \frac{\exp(\bar{A}_{ij})}{\sum \exp(\bar{A}_{ik})} \tag{6}$$

The sum of attention weights from each node to its neighbours is ensured to be 1. In the fifth step, structure-weighted aggregation of value information is performed:

$$H_i = \sum_j A_{ij} V_j \tag{7}$$

The output matrix $H \in R^{N \times D_V}$ is defined as the structure-aware representation of each atom.

Through above described process, simultaneous encoding of bond-length and bond-angle dependencies while preserving local symmetry information were enabled. All descriptor operators (SE_E2, SE_E2_A and attention-augmented variants) are implemented through the native descriptor and model-definition modules in the DeePMD-kit framework, which internally handles descriptor embedding, environment mapping and neural network fitting without external coding intervention.

IV. Fitting interatomic potentials of SiC

4.1. Theoretical foundation of deep potential

The core idea of the deep potential method is to use atomic-level neural network potentials. Complex many-body interactions are decomposed into a sum of energy contributions from individual atoms. For a system containing N atoms, the total energy is expressed as the sum of atomic energies:

$$E_{total} = \sum_{i=1}^{N} E_i \tag{8}$$

The energy of a single atom, E_i, is determined uniquely by its surrounding local atomic environment:

$$E_i = f(\varsigma_i) \tag{9}$$

The construction of the local environment is required to remain physically invariant under translation and rotation. To achieve this, an environment matrix R_i is defined for each atom i:

$$R_i = \{s(r_{ji}) \cdot r_{ji} | j \neq i, r_{ji} < r_c\} \tag{10}$$

where $s(r_{ji})$ is a smooth weighting function. It is used to describe the contribution weight of neighbouring atom j to the central atom i:

$$s(r_{ji}) = \frac{1}{2}\left[\cos\left(\frac{\pi \cdot r_{ji}}{r_c}\right) + 1\right], r_{ji} < r_c \tag{11}$$

The function smoothly decays to zero near the cut-off radius r_c. This ensures that the potential is differentiable over the entire domain. However, R_i only possesses translational invariance. To achieve symmetry under translation, rotation, and permutation of identical atoms, R_i is projected into the chemical descriptor space through a feature mapping function:

$$\varsigma_i = \Phi(R_i) \tag{12}$$

Under different descriptor construction methods, information is extracted from various components of R_i and used as input to the neural network. The potential efficiently captures the non-linear relationship between the local environment and atomic energy while preserving physical symmetries.

4.2. Execution workflow of DP-GEN

After fitting the deep potential for the SiC system, the initial deep learning potential shows significant deviations in energy and force predictions for some local structures during molecular dynamics simulations. It cannot meet the requirements of high-precision modelling. To improve the applicability and generalization of the potential, the DP-GEN framework, based on an active learning strategy, is introduced. Weak regions in the potential energy model are continuously discovered and corrected through iterative sampling and high-precision labelling. Figure 3 shows a complete DP-GEN cycle in the SiC system, illustrating the identification of potential defects and the optimization of the deep potential.

In the initial dataset shown in Fig. 3b, the initial configurations are generated by calling AIMD calculations in the CP2K software. During the simulation, bond lengths and angles between C atoms and Si atoms

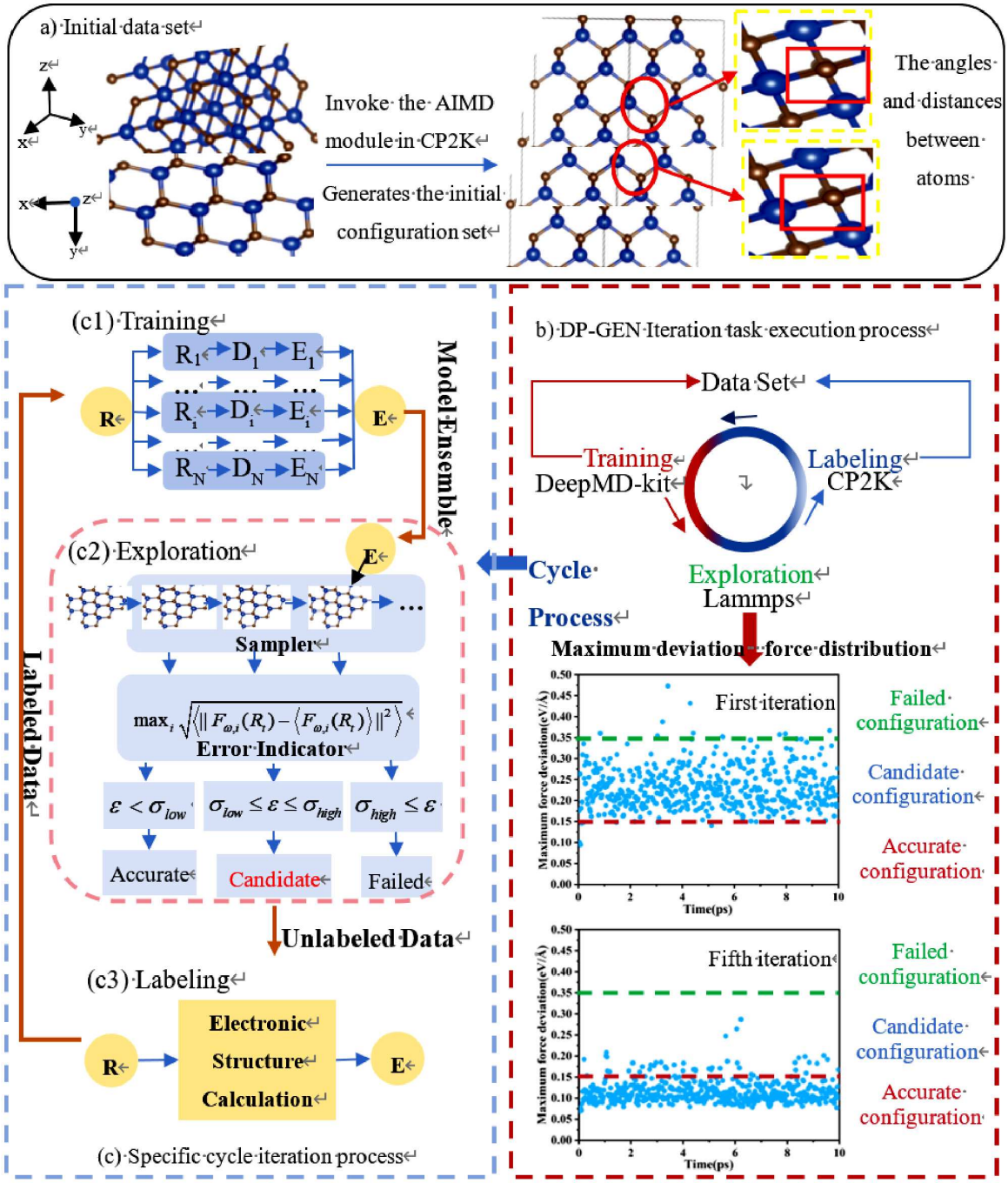

Figure 3. Iterative process of DP-GEN for optimizing the SiC potential

change continuously until the energy reaches equilibrium. These configurations with different bond lengths and angles are used to construct the training dataset for the deep learning potential. However, some invalid configurations exist in the initial dataset. They are corrected, and the DP-GEN generator is used to address this issue. DP-GEN is a parallel learning process. Each iteration includes three main steps: training, exploration, and labelling. The training dataset obtained from DFT calculations is first initialized with different potentials. Relevant functions are defined using the DeePMD-kit simultaneous-training parameters. Next, in the exploration stage, the configuration space is expanded. MD simulations are performed in LAMMPS using the potentials obtained from training and the specified initial structures. The resulting configurations are screened based on the standard deviation of atomic forces. Finally, in the labelling step, the selected configurations receive DFT single-point calculations to obtain forces and energies. These new configurations are added to the training dataset for a new round of training. The iterative cycle is shown in Fig. 3a. In the training step, a deep neural network (DNN) maps the local atomic environment to the atomic energy E_i, and the total sys-

tem energy E is obtained by summation. The DNN effectively captures the dependence of atomic energy on local atomic coordinates. Next is the exploration step, which consists of an efficient sampler and an error indicator. The sampler aims to explore the configuration space effectively and uses the DP model to evaluate the potential and atomic forces. The maximum force deviation index is defined as the maximum standard deviation ε of atomic forces F_i predicted by the DP model:

$$\varepsilon = \max \sqrt{\|F_i - \langle F_i \rangle\|^2} \tag{13}$$

During training, the average of all deep potential model predictions is used as the reference for model output. At the beginning of training, a wide deviation range can be set. The initial upper limit was $\sigma_{high} = 0.35\,\text{eV Å}^{-1}$ and the lower limit was $\sigma_{low} = 0.15\,\text{eV Å}^{-1}$. This range is dynamically adjusted according to the model convergence to improve accuracy. Configurations with maximum force deviation ε within $\sigma_{low} < \varepsilon < \sigma_{high}$ are defined as candidate configurations. When the maximum force deviation of all sampled configurations satisfies $\varepsilon < \sigma_{low}$, the DP-GEN task is terminated. If the maximum force deviation is $\varepsilon > \sigma_{high}$, the predicted forces deviate excessively; the total system energy is too high, causing the configurations to fail to converge in the first-principles calculations. These configurations are then defined as failed configurations. The setting of σ_{low} is determined by the peak position of the maximum force deviation distribution curve. If the distribution peak is on the left of σ_{low}, the lower limit is set reasonably. If the peak is on the right or the distribution range is too wide, the upper and lower thresholds need to be adjusted. Otherwise, it is difficult to construct a high-precision potential energy model.

4.3. Validation of model computational efficiency

In multiscale materials simulations, the choice of potential directly affects the spatial and temporal scales of the simulations. To balance computational speed and physical accuracy, a deep learning-based deep potential (DP) is constructed for silicon carbide. Its performance is systematically evaluated. The computational speed and accuracy results are shown in Fig. 4.

To systematically evaluate the computational efficiency of different potentials in molecular dynamics simulations of the SiC system, the simulation performance of DFT, classical Tersoff potential, and deep learning-based DeepMD potential are compared under the same computational environment. MD simulations are run for 100 steps at 1000 K with a time step of 1 fs. The number of simulation steps completed per second is measured for the three potentials. The results are shown in Fig. 4. DFT, as an *ab initio* method, has extremely high computational cost and completes only about 0.016 steps per second. The Tersoff potential achieves about 8700 steps per second due to its simple analytic form, making it the fastest among the three. DeepMD achieves about 34 steps per second while maintaining physical accuracy. Compared with DFT, DeepMD is approximately three orders of magnitude faster on the same CPU. Although slightly slower than Tersoff, the data-driven mechanism of DeepMD provides better generalization and stronger physical adaptability.

Furthermore, to compare the structural description capabilities of the three potentials, the radial distribution function $g(r)$ of SiC calculated by each method is shown on the right side of the figure. The DFT curve is used as the reference. The DeepMD prediction closely overlaps with DFT, showing good agreement in the position and intensity of the main peak. This indicates that it accurately reproduces interatomic structural features. The

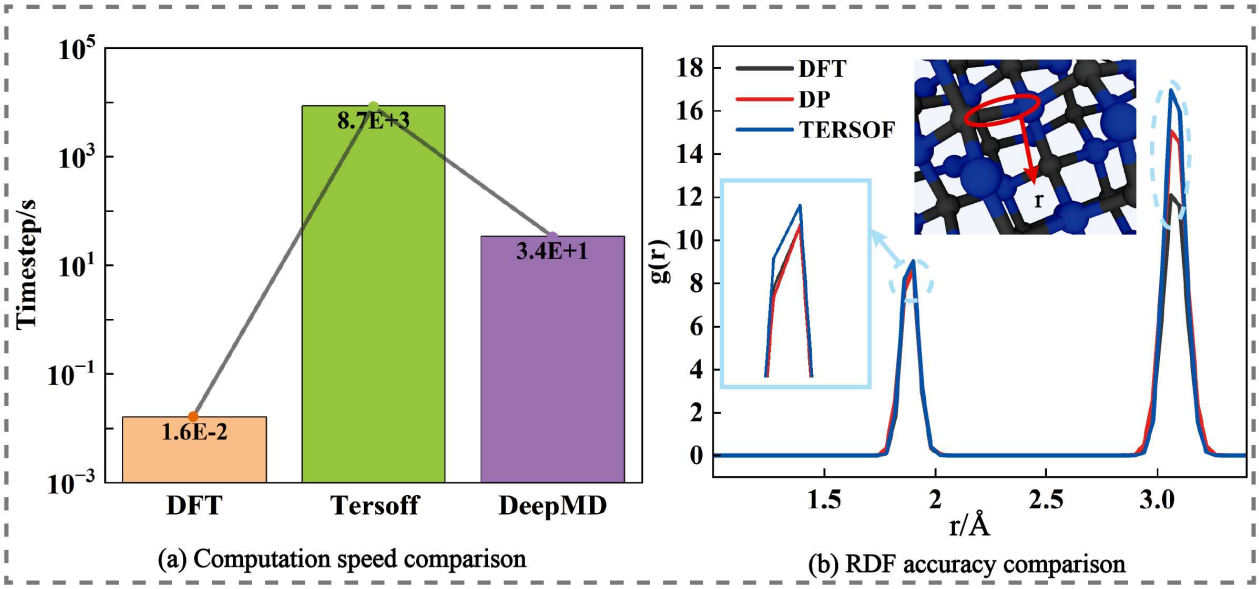

Figure 4. Analysis of computational efficiency

Tersoff potential shows obvious deviations in the first nearest-neighbour distance and higher-order peaks, reflecting its limitations in describing short- and medium-range atomic arrangements. Considering both computational efficiency and structural accuracy, the DeepMD potential maintains high performance while achieving near-DFT structural prediction accuracy. It provides a feasible approach for a large-scale, high-precision simulations of SiC materials.

V. DFT and machine learning potentials

5.1. *Comparison of energy and force prediction accuracy across multiple models*

The prediction accuracy of the constructed deep potential (DP) model for silicon carbide on atomic energy and force at medium and high temperatures is systematically evaluated. Molecular dynamics relaxation processes are performed at different temperatures. Five temperatures were selected: 400, 600, 800, 1100 and 1300 K. From each temperature, a testing dataset with 200 time steps is sampled. The results are shown in Fig. 5.

The upper part of Fig. 5 shows the model evaluation at 600 K. The first panel (Fig. 5a) presents the comparison between the per-atom energy predicted by the DP model and the DFT reference. The data are distributed along the ideal fitting line ($y = x$). No large systematic deviation is observed. The enlarged view shows that the energy errors are mainly concentrated within ±0.002 eV, and the distribution forms a narrow peak. High accuracy and stability of the model at low temperature are demonstrated. The second panel (Fig. 5b) shows the force prediction in three directions. The predicted values of F_x, F_y and F_z match the DFT results well. The error frequency distributions in all directions are similar. The errors are mainly located within ±0.01 eV/Å. Good isotropy of force prediction is demonstrated. Panels, presented in Figs. 5c and 5d, show the energy error distributions and the variation of force RMSE at different temperatures. As the temperature increases from 400 to 1300 K, the error peaks of energy remain close to zero. Slightly longer tails appear at higher temperatures. The overall accuracy remains stable. The RMSE of force increases slightly from about 0.004 eV/Å at 400 K to 0.00986 eV/Å at 1300 K. Strong robustness of

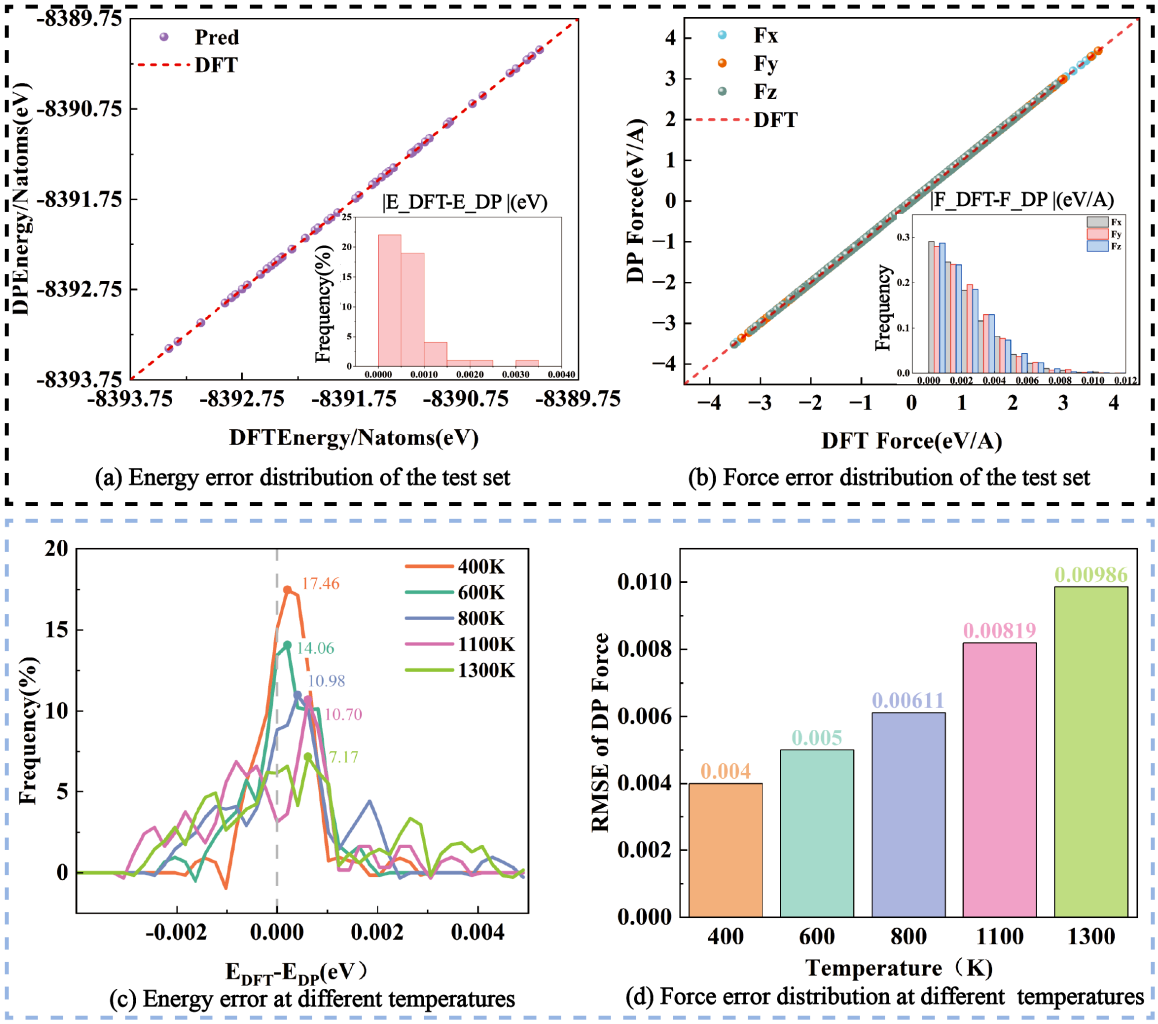

Figure 5. Error distribution of energy and force predicted by the DP model

force prediction under enhanced thermal disturbance is demonstrated. In summary, the DP potential shows good generalization accuracy below 1300 K. The errors are smallest in the range of 400–800 K. The potential is applicable to large-scale dynamic simulations of SiC at medium and high temperatures.

5.2. *Bond length and angle statistics and local distortion characteristics*

Due to the differences of interaction description in different potentials, the local distribution of atomic forces and structural response show clear differences. The statistical features of bond length and bond angle are influenced. To further verify the accuracy of the constructed deep potential (DP) in structural prediction, DFT, classical empirical potential (Tersoff), and DP potential are compared in the description of atomic structure in the SiC system. The fitting of bond length and bond angle distributions is evaluated. The local structural distortion at the atomic scale is analysed. The comparison provides direct evidence for the ability of different models to reproduce microscopic structures. The results are shown in Fig. 6.

In molecular dynamics simulations, the interactions between atoms directly affect the structural evolution of the system. The differences are mainly reflected in the statistical distributions of bond length and bond angle. To evaluate the capability of different potentials in describing atomic-scale structural features, the trajectories of SiC generated by first-principles (DFT), deep learning potential (DP), and classical empirical potential (Tersoff) are analysed statistically. As shown in Fig. 6a, the bond length distribution mainly lies in the range of 1.8 to 2.1 Å. Obvious differences are observed in the predictions of different potentials. The bond length distribution predicted by the Tersoff potential shows a shift of the main peak and a broader tail compared to DFT. A systematic error in local structural constraints is indicated. In contrast, the bond length distribution predicted by the DP potential matches DFT closely in peak position, curve shape, and distribution width. The consistency demonstrates that local interactions and bond energy surfaces are accurately described. The bond angle distributions show that the average values of the three methods concentrate between 108° and 112°. The Tersoff potential gives a shifted peak position, which indicates its limitation in describing local angular tension. In contrast, the DP potential shows strong agreement with DFT in peak position and distribution shape, with only slight differences at the edges. This agreement further confirms its accuracy in reproducing the tension of Si–C bonds and the spatial arrangement of

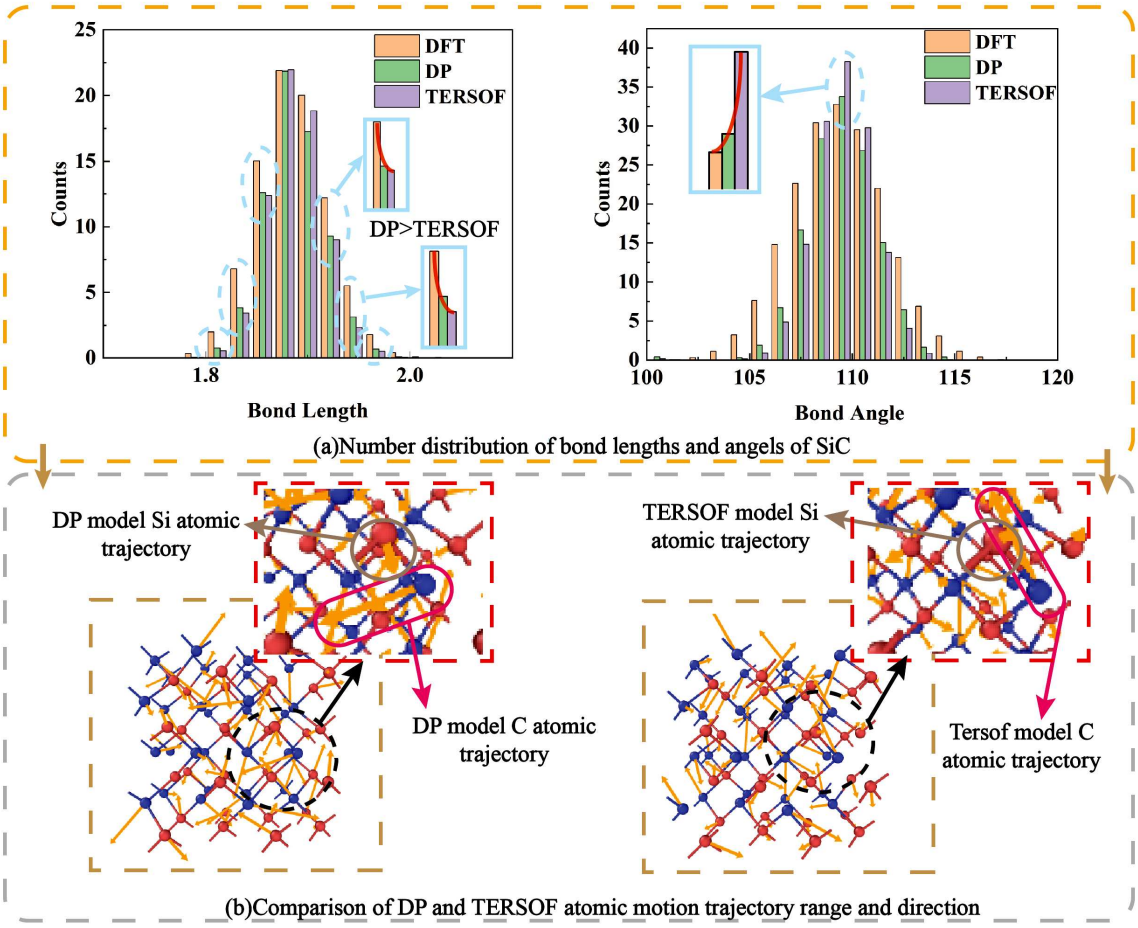

Figure 6. Comparison of bond length distribution, bond angle distribution and atomic trajectories of SiC structures

atoms. To further reveal the difference in atomic dynamics, Fig. 6b presents the trajectory distributions of typical Si and C atoms in the SiC system. Blue regions represent C atoms, and red regions represent Si atoms. The atomic trajectories predicted by the Tersoff potential are more dispersed, with a wide distribution range and irregular patterns. This result indicates large fluctuations of predicted atomic forces, which may cause strong thermal disturbances in the system. In contrast, the atomic trajectories predicted by the DP potential are localized and symmetric, with narrower ranges of motion. A stable motion on the potential energy surface is indicated. Especially for C atoms, the DP potential accurately restricts high-frequency vibration while maintaining thermal stability. This result shows that the microscopic thermal motion of SiC at high temperatures is reasonably described.

Overall, the DP potential shows much closer agreement with DFT in trajectory evolution and atomic force prediction compared with the Tersoff potential. A solid basis for high-accuracy dynamical simulations is provided.

VI. Simulation of SiC behaviour

To investigate the effect of temperature on the subsurface damage evolution in silicon carbide, molecular dynamics nanoindentation simulations were performed using the deep learning potential (DeePMD). The SiC molecular dynamics model was constructed in

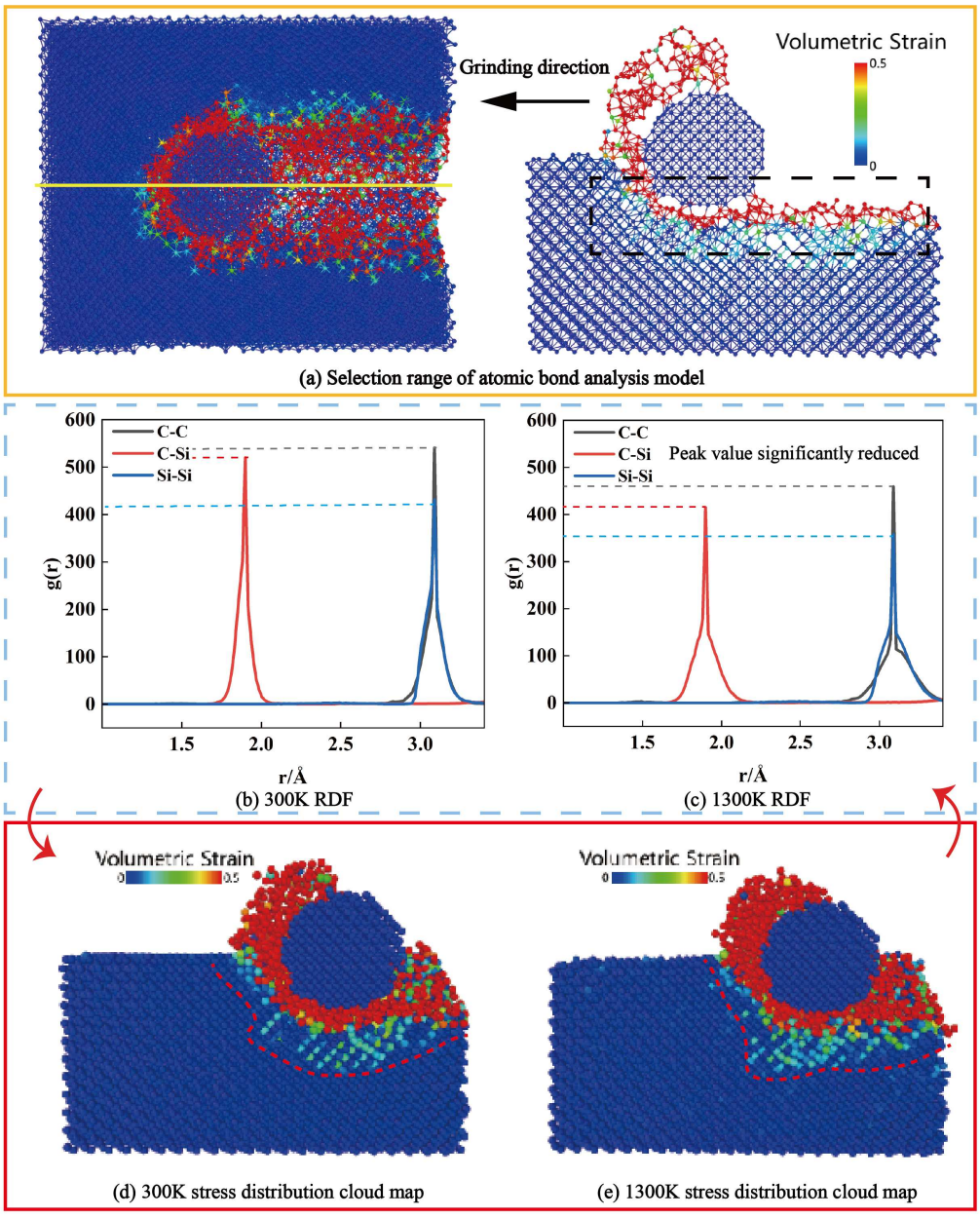

Figure 7. Atomic-scale damage evolution of silicon carbide during grinding under different temperature conditions

LAMMPS. The main body of the model adopts a hexagonal SiC lattice, and a rigid spherical SiC indenter is placed above it. The simulation system is divided into three layers along the z-axis from bottom to top: i) a 0.5 nm boundary layer, ii) a 0.5 nm thermostat layer and iii) a 4 nm Newton layer. The velocities of atoms in the boundary layer are fixed to suppress boundary effects. The thermostat layer is used to maintain a stable system temperature and realize heat exchange. The Newton layer serves as the main region for force response. Periodic boundary conditions are applied to prevent edge atom loss. The indenter is pressed into the specimen along the z-axis at a fixed speed. The maximum indentation depth is set to 1.5 nm. The surface damage of both components is analysed as shown in Fig. 7.

Figure 7a shows the model selection region for bond breakage analysis during nanoscale grinding and the corresponding grinding direction setup, which is used as the basis for subsequent bond damage statistics. Figures 7b and 7c show the volumetric strain distribution maps of the SiC workpiece during nanoindentation when the indenter penetration depth reaches 1.5 nm at 300 and 1300 K, respectively. The region outlined by the red dashed line indicates the significant damage caused by the indenter. At 300 K (Fig. 7d), local atoms near the indenter exhibit noticeable accumulation, and the damage region is relatively concentrated while the structure maintains a certain degree of order. At 1300 K (Fig. 7e), atomic activity is enhanced by thermal excitation, leading to a significant expansion of the damage region and obvious local structural disruption and disorder. Under high-temperature conditions, atoms slide and rearrange more easily, and the integrity of the microstructure decreases significantly.

Figures 7b and 7c show the radial distribution function (RDF) comparisons of C–C, C–Si and Si–Si atomic pairs under the same penetration depth (1.5 nm) at different temperatures. The first-neighbour peak positions remain unchanged at approximately 2.0 Å (C–Si), 2.5 Å (C–C) and 3.1 Å (Si–Si). However, at 1300 K, the RDF peak intensity of C–Si bonds decreases significantly, indicating a strong reduction in local order between these atoms. The RDF curves of C–C and Si–Si pairs also show reduced peak heights and broadened peak shapes, reflecting weakened interatomic interactions, enhanced structural relaxation, and increased local bond breakage and rearrangement. These results further confirm that SiC workpieces are more prone to subsurface damage and structural failure under high-temperature conditions.

VII. Conclusions

This study constructs a structure-energy dataset for SiC under high-temperature conditions based on the first-principles calculations. An initial interatomic potential is built using an improved DeepMD deep neural network framework. A multi-head attention mechanism is introduced into the descriptor module to enhance the model's perception of complex atomic interactions. The DP-GEN adaptive iterative workflow is designed to optimize sampled configurations using an active learning strategy. The model's capability to describe atomic interactions under high-temperature structural diversity and deformation fields is gradually improved. Finally, a high-precision SiC deep learning potential suitable for simulating high-temperature grinding and indentation behaviour is obtained. Test results show that the potential predicts atomic energies with an RMSE of about 0.42 meV/atom and interatomic forces with an RMSE of 49 meV/Å. The computational efficiency is increased by 5–6 orders of magnitude compared to DFT, and good generalization performance is maintained under high-temperature and high-strain conditions. Analyses of radial distribution functions and local strain distributions further confirm the accuracy of the deep learning potential in capturing SiC structural responses at different temperatures.

The attention-based SiC deep learning potential proposed in this study effectively addresses the limitations of traditional empirical potentials (such as Tersoff and MEAM) in modelling high-temperature, large-deformation processes and overcomes the low computational efficiency of DFT, which cannot support nanosecond-scale dynamic simulations. Using this potential, the grinding and nano-indentation processes of SiC workpieces under high-temperature conditions with a diamond tool are simulated. The results show that, as the temperature increases, the atomic structure inside the workpiece undergoes more severe reconstruction, the surface accumulation and slip defects become more pronounced, and thermal softening enhances both the volumetric strain and local potential energy in the indentation region. These findings provide theoretical support for understanding the micro-damage behaviour and failure mechanisms of SiC at high temperatures and establish a potential basis for subsequent multi-scale simulations using the DP potential, such as crack nucleation and propagation or friction-induced damage evolution.

Acknowledgement: This study is sponsored by the projects found by the Jiangxi Provincial Department of Education project: GJJ2500907; GJJ2500902; GJJ2500904 to which the authors are very grateful. The authors also sincerely thank the editor and the anonymous reviewers for their valuable and useful comments to improve our manuscript.

References

1. C. Mi, Y. Wang, Q. Guo, Q. Zhang, "Research progress on the preparation and application of nano silicon carbide", *Hans J. Chem. Eng. Technol.*, **13** [5] (2023) 362–372.
2. S. Singh, K. Rathi, K. Pal, "Synthesis, characterization of graphene oxide wrapped silicon carbide for excellent mechanical and damping performance for aerospace application", *J. Alloys Compd.*, **740** (2018) 436–445.

3. D.G. Senesky, B. Jamshidi, K.B. Cheng, A.P. Pisano, "Harsh environment silicon carbide sensors for health and performance monitoring of aerospace systems: A review", *IEEE Sensors J.*, **9** [11] (2009) 1472–1478.
4. F. Monteverde, L. Scatteia, "Resistance to thermal shock and to oxidation of metal diborides-SiC ceramics for aerospace application", *J. Am. Ceram. Soc*., **90** [4] (2007) 1130–1138.
5. M. De Napoli, "SiC detectors: A review on the use of silicon carbide as radiation detection material", *Front. Phys*., **10** (2022) 898833.
6. D.-R. Sun, G. Wang, Y. Li, Y. Yu, C. Shen, Y. Wang, Z. Lu, "Laser drilling in silicon carbide and silicon carbide matrix composites", *Opt. Laser Technol*., **170** (2024) 110166.
7. T. König, M. Galetz, B. Albert, "Application of the pack cementation process on SiC/SiC ceramic matrix composites", *J. Eur. Ceram. Soc*., **41** [16] (2021) 101–112.
8. Y. Gao, Y. Chen, P. Ge, L. Zhang, W. Bi, "Study on the subsurface microcrack damage depth in electroplated diamond wire saw slicing SiC crystal", *Ceram. Int.*, **44** [18] (2018) 22927–22934.
9. X. Hui, Y. Xu, Y. Hou, "A coupled micro–meso-scale study on the damage mechanism of 2D SiC/SiC ceramic matrix composites", *Mech. Adv. Mater. Struct.*, **28** [20] (2021) 2083–2095.
10. B.V. Tanikella, K.A. Gruss, R.F. Davis, R.O. Scattergood, "Indentation and microcutting fracture damage in a silicon carbide coating on an Incoloy substrate", *Surf. Coat. Technol*., **88** [1-3] (1997) 119–126.
11. M.T. Rad, M. Foroutan, "Wettability of tetrahexcarbon: MD, DFT, and AIMD approaches", *Langmuir*, **39** [23] (2023) 8279–8296.
12. X. Wang, Z.-J. Liu, J.-S. Feng, M.-R. Chen, L. Li, X.-W. Sun, F. Tian, "Construction and application of deep learning potential for CaO under high pressure", *Comput. Mater. Sci*., **244** (2024) 113154.
13. Y. Liu, H. Wang, L. Guo, Z. Yan, J. Zheng, W. Zhou, J. Xue, "Deep learning inter-atomic potential for irradiation damage in 3C-SiC", *J. Nucl. Mater*., **233** (2024) 112693.
14. C.-J. Ding, Y.-W. Lei, X.-Y. Wang, X.-L. Li, X.-Y. Li, Y.-G. Zhang, Y.-C. Xu, C.-S. Liu, X.-B. Wu, "A deep learning interatomic potential suitable for simulating radiation damage in bulk tungsten", *Mater. Today Commun*., **6** [2] (2024) 304–322.
15. J. Zeng, D. Zhang, D. Lu, P. Mo, Z. Li, Y. Chen, M. Rynik, L. Huang, Z. Li, S. Shi, Y. Wang, H. Ye, P. Tuo, J. Yang, Y. Ding, Y. Li, D. Tisi, Q. Zeng, H. Bao, Y. Xia, J. Huang, K. Muraoka, Y. Wang, J. Chang, F. Yuan, S.L. Bore, C. Cai, Y. Lin, B. Wang, J. Xu, J.X. Zhu, C. Luo, Y. Zhang, R.E.A. Goodall, W. Liang, A.K. Singh, S. Yao, J. Zhang, R. Wentzcovitch, J. Han, J. Liu, W. Jia, D.M. York, E. Weinan, R. Car, L. Zhang, H. Wang, "DeePMD-kit v2: A software package for deep potential models", *J. Chem. Phys*., **159** [5] (2023) 054801.
16. Y. Zhang, H. Wang, W. Chen, J. Zeng, L. Zhang, H. Wang, E. Weinan, "DP-GEN: A concurrent learning platform for the generation of reliable deep learning based potential energy models", *Comput. Phys. Commun*., **253** (2020) 107206.
17. A.V. Savchenkov, "Designing three-dimensional models that can be printed on demand and used with students to facilitate teaching molecular structure, symmetry, and related topics", *J. Chem. Educ*., **97** [6] (2020) 1682–1687.
18. J.P. Rino, I. Ebbsjö, P.S. Branicio, R.K. Kalia, A. Nakano, F. Shimojo, P. Vashishta, "Short- and intermediate-range structural correlations in amorphous silicon carbide: A molecular dynamics study", *Phys. Rev. B*, **70** [4] (2004) 045207.
19. M.J. Islam, "A comprehensive investigation on the physical properties of SiC polymorphs for high-temperature applications: A DFT study based on GGA and hybrid HSE06 exchange correlation functionals", *Nucl. Mater. Energy*, **38** (2024) 101631.
20. E. Bekaroglu, M. Topsakal, S. Cahangirov, S. Ciraci, "First-principles study of defects and adatoms in silicon carbide honeycomb structures", *Phys. Rev. B*, **81** [7] (2010) 075433.